# Numerical Simulation of Proton Distribution with Electric Double Layer in Extended Nanospaces

**ARTICLE** *in* ANALYTICAL CHEMISTRY · APRIL 2013

Impact Factor: 5.64 · DOI: 10.1021/ac400001v · Source: PubMed



**6 AUTHORS**, INCLUDING:

Yutaka Kazoe
The University of Tokyo
**58** PUBLICATIONS **243** CITATIONS
SEE PROFILE

Ruey-Jen Yang
National Cheng Kung University
**164** PUBLICATIONS **2,757** CITATIONS
SEE PROFILE

analytical chemistry

Article

pubs.acs.org/ac

# Numerical Simulation of Proton Distribution with Electric Double Layer in Extended Nanospaces

Chih-Chang Chang,[†,‡] Yutaka Kazoe,[†] Kyojiro Morikawa,[†] Kazuma Mawatari,[†] Ruey-Jen Yang,[‡] and Takehiko Kitamori*[,†]

[†]Department of Applied Chemistry, School of Engineering, The University of Tokyo, 7-3-1 Hongo, Bunkyo, Tokyo 113-8656, Japan

[‡]Department of Engineering Science, National Cheng Kung University, Tainan 70101, Taiwan

**ABSTRACT:** Understanding the properties of liquid confined in extended nanospaces (10−1000 nm) is crucial for nanofluidics. Because of the confinement and surface effects, water may have specific structures and reveals unique physicochemical properties. Recently, our group has developed a super resolution laser-induced fluorescence (LIF) technique to visualize proton distribution with the electrical double layer (EDL) in a fused-silica extended nanochannel (Kazoe, Y.; Mawatari, K.; Sugii, Y.; Kitamori, T. *Anal. Chem.* **2011**, *83*, 8152). In this study, based on the coupling of the Poisson−Boltzmann theory and site-dissociation model, the effect of specific water properties in an extended nanochannel on formation of EDL was investigated by comparison of numerical results with our previous experimental results. The numerical results of the proton distribution with a lower dielectric constant of approximately 17 were shown to be in good agreement with our experimental results, which confirms our previous observation showing a lower water permittivity in an extended nanochannel. In addition, the higher silanol deprotonation rate in extended nanochannels was also demonstrated, which is supported by our previous results of NMR and streaming current measurements. The present results will be beneficial for a further understanding of interfacial chemistry, fluid physics, and electrokinetics in extended nanochannels.

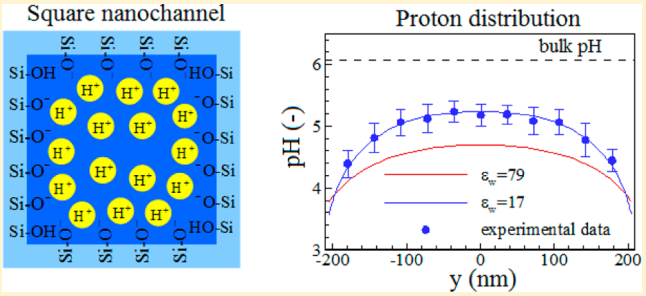


Fluid and species transport in submicrometer confinements are a common issue in many classical fields, such as biology, geology, membrane science, separation science, and colloid science, etc., which was referred to as "classical nanofluidics".[1] As nanotechnology has been rapidly developed, well-designed and controlled nanochannels provide a more ideal fluidic system than classical nanofluidics to study the nanoscale transport phenomena and explore new science in a precise manner. This "new nanofluidics"[2] will benefit to rapidly develop new functional elements and tools for the fields of microbiochemical analytical systems,[3] bionics,[4,5] water purification,[6] and energy harvesting.[7−9] As the dimension of space downscales to the nanometer regime, behaviors of liquid molecules may be very different from those in bulk due to the confinement and surface effects. Therefore, understanding physicochemical properties of liquid confined in nanospaces is an essential issue prior to the applications.

In the past decades, a variety of theoretical and experimental investigations have demonstrated that the water molecules confined in sub-10 nm spaces such as carbon nanotubes and nanoporous silica reveal the specific features that are not observed in bulk,[10−14] e.g., formation of icelike structure on the surface (i.e., adsorbed water phase), depression of freezing-point, and slowing down of water molecule dynamics. This generally was attributed to the orientational order of water molecules confined on the several-nanometers scale. Recently, Duan and Majumdar[15] demonstrated that the proton mobility in 2 nm silica nanochannels is about 3−4 times the bulk value. It was inferred that the enhancement of proton mobility is due to the presence of the oriented structure of water molecules confined in nanospaces, which is beneficial for proton hopping (i.e., Grotthuss mechanism).

On the other hand, a 10−1000 nm space termed as "extended nanospace" is expected to be an attractive space size for implementing novel nanofluidic devices in the fields of analytical chemistry and single biomolecules analysis.[3,16,17] The extended nanospace is a transition regime of liquid molecular behavior from single molecules to a bulk condensed phase, and fluid physics and chemistry still remain to be further clarified. More recently, our nuclear magnetic resonance (NMR) studies of confined water dynamics in fused-silica extended nanochannels showed a size-dependence of the proton exchange rate in water, which is greatly enhanced below the space size of approximately 800 nm.[18,19] From these observations, we hypothesized that there is an intermediate phase between the adsorbed water phase and bulk phase in extended nanochannels, which was referred to as the proton-transfer phase of loosely coupled water molecules by hydrogen bond within

**Received:** January 1, 2013
**Accepted:** April 2, 2013
**Published:** April 2, 2013

   dx.doi.org/10.1021/ac400001v | *Anal. Chem.* 2013, 85, 4468−4474

several tens of nanometers from the silica surface. This hypothesis for the specific structure of water confined in hydrophilic extended nanochannels, namely, a"three phase model", was further demonstrated by our other experimental observations showing higher proton diffusivity,[20] lower permittivity,[21] and higher water viscosity.[21,22] Accordingly, the electrical double layer (EDL) comprised of the Stern layer and diffuse layer formed in the vicinity of a charged surface,[23] as schematically shown in Figure 1, is expected to be affected by

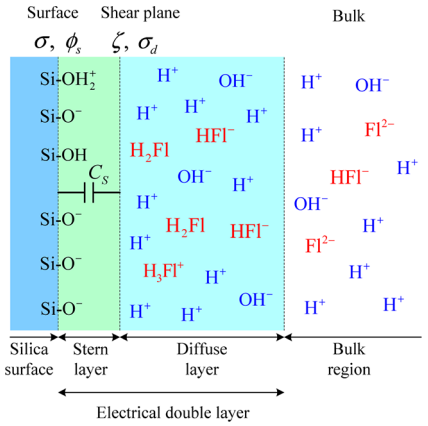


**Figure 1.** Schematic illustration of electrical double layer consisting of a Stern layer and a diffuse layer formed near a silica surface bearing a surface charge density $\sigma$ and a surface potential $\phi_s$. $\zeta$ is the electrical potential at the shear plane and $\sigma_d$ is the charge density in diffuse layer. $C_s$ is the Stern layer capacitance. Note that the ions of $H_3Fl^+$, $HFl^-$, and $Fl^{2-}$ are produced from the dissociation of fluorescein ($H_2Fl$) in water.

the specific structure of water molecules confined in extended nanochannels. Since the EDL thickness (i.e., Debye length) of approximately 1−300 nm is comparable to the size of extended nanospaces and the thickness of the proton-transfer phase, it will have a significant influence on the extended nanoscale electrokinetic (EK) phenomena, including electroosmotic flow (EOF) and streaming current/potential.

In previous extended nanoscale studies for EDL, most were focused on the macroscopic investigations of EK phenomena in nanochannels and nanopores, such as ion-depletion/ion-enrichment near the micronanospace interface,[24] nonlinear EOF outside of nanospaces,[25] ionic current reification,[26−28] streaming current/potential,[29−33] electrical conductance measurement,[34,35] and electrokinetic species separation.[36,37] van den Heyden et al.[29] and Jensen et al.[34] employed the Poisson−Boltzmann (PB) theory combined with the site-dissociation model to predict the streaming current and electrical conductance in silica nanochannels on an assumption of the bulk properties of water, e.g., viscosity, permittivity, and proton mobility. Pennathur and Santiago[36,37] predicted the electrokinetic separation by ion valence (EKSIV) in nanochannels using the PB theory with the bulk properties. On the other hand, as mentioned above, our recent experimental results have showed specific water properties in fused-silica nanochannels. In addition, the streaming current measurements in sub-800 nm nanochannels revealed that the fused-silica surface bears the negative surface charges at a pH value below the well-known point-of-zero-charge (PZC) of the silanol group.[38] This implies that surface chemistry in extended nanochannels may be affected by the specific features of confined water. In order to achieve a better understanding of the behavior of confined water in nanochannels and EDL affected by the specific structure, microscopic observations of EDL in extended nanospaces are strongly required.

Most recently, our group has developed a method to directly measure the ion distribution in extended nanochannels using a super resolution-laser induced fluorescence method by a stimulated emission depletion (STED) microscopy system.[39] The proton distributions in a 400 nm fused-silica extended nanochannel were obtained for the first time. The proton concentration becomes nonuniform and 19 times higher than the bulk when the extended nanochannel was filled with water. On the basis of the results, under the assumption of bulk liquid properties, Anzo and Okada[40] argued that the PB theory (i.e., Gouy−Chapmann model) cannot successfully interpret our measured data of proton distribution in extended nanochannels filled with pure water. They supposed that the EDL overlapping restricts the applicability of the PB theory. On the other hand, we claimed that microscopic liquid structure in extended nanochannels should be further considered in the EDL theory.[41]

According to electrostatic theory, it is well-known that the electrostatic field ($\mathbf{E}$) is governed by the Poisson equation as follows

$$\nabla\cdot(\varepsilon_w\varepsilon_0\mathbf{E}) = \rho_e \tag{1}$$

where $\varepsilon_w$ is the dielectric constant of water and $\varepsilon_0$ is the vacuum permittivity. $\rho_e$ is the net volume charge density. It is seen that the electrical potential and charge distribution within EDL will be affected by the water permittivity that is strongly related to the structure of water molecules confined in extended nanospaces. Our previous study has demonstrated that the dielectric constant of water confined in the fused-silica extended nanochannel becomes lower than the bulk by the time-resolved fluorescence measurements.[21] In this study, we implement a numerical estimation based on the PB theory coupled with the chemical equilibrium model to investigate the EDL and proton distribution of pure water in a fused-silica extended nanochannel. The influence of the specific properties of confined water and surface chemistry on the formation of EDL is discussed by comparison of numerical results with our experimental results obtained by STED microscopy. This study will provide an insight into interfacial chemistry, fluid physics, and electrokinetics at the extended nanoscale.

## NUMERICAL MODEL

**Governing Equation and Boundary Condition.** A fluidic system consisting of a microchannel part and a nanochannel part was used to study the proton distribution inside an extended nanochannel.[39] Consider the equilibrium condition between ionic solution in the microchannel and that within the nanochannel and assume that the ion is a point charge, then the ion distribution ($c_i$) in the nanochannel can be described by the following Boltzmann distribution even if EDL overlaps[42,43]

$$c_i = c_i^{\infty}\exp\left(-\frac{z_iF\phi}{RT}\right) \tag{2}$$

where $c_i^{\infty}$ is the concentration of type-$i$ ion at the bulk (or the microchannel part) and $z_i$ is the valence of type-$i$ ion. $\phi$ is the EDL potential. $F$, $R$, and $T$ are the Faraday constant, the gas constant, and the absolute temperature, respectively. Substitut-


dx.doi.org/10.1021/ac400001v | Anal. Chem. 2013, 85, 4468−4474

ing the net volume charge density, $\rho_e = F\sum_i z_i c_i$, into eq 1, yields the following PB equation for EDL field

$$\nabla\cdot(\varepsilon_w\varepsilon_0\nabla\phi) = -F\sum_i z_i c_i^{\infty}\exp\left(-\frac{z_i F\phi}{RT}\right) \quad (3)$$

The corresponding boundary condition on the charged wall is given as $\mathbf{n}\cdot(\varepsilon_w\varepsilon_0\nabla\phi)|_{wall} = \sigma$, where $\sigma$ is the surface charge density. In the experiments, fluorescein ($C_{20}H_{12}O_5$ or $H_2Fl$) was used as a pH indicator to visualize the proton distribution in the extended nanochannel.[39] The chemical reaction schemes used to calculate the species concentration within pure water are listed in Table 1. The concentration of the dissolved ions in the bulk solution was calculated in accordance with the principles of mass conservation and electroneutrality. Moreover, the site-dissociation model of the silanol group (SiOH) on the silica surface, as shown in Figure 1, was employed as the boundary condition in our numerical modeling. The surface charge density based on the site-dissociation model is given as[53]

**Table 1. Chemical Reaction Schemes and Equilibrium Constants Used in the Numerical Modeling**

| chemical family | reaction scheme | equilibrium constant (p$K$) |
|---|---|---|
| water ($H_2O$) | $H_2O \leftrightarrow OH^- + H^+$ | 14.00 |
| fluoresceion ($H_2Fl$) | $H_3Fl^+ \leftrightarrow H_2Fl + H^+$ | 2.13[a] |
| | $H_2Fl^+ \leftrightarrow HFl^- + H^+$ | 4.44[a] |
| | $HFl^- \leftrightarrow Fl^2 + H^+$ | 6.36[a] |
| silanol (SiOH) | $SiOH_2^+ \leftrightarrow SiOH + H^+$ | $pK_{a1}$[b] |
| | $SiOH \leftrightarrow SiOH + H^+$ | $pK_{a2}$[c] |

[a]From ref 44. [b]The $pK_{a1}$ value of silanol group is given as −1.9 from refs 45 and 46. [c]The $pK_{a2}$ value of the silanol group is a fitting value in this study, which was reported in the range of 5.8−9.86 in refs 45−52.

$$\sigma = e\Gamma\frac{\delta\sinh[F(\phi_N - \phi_s)/RT]}{1 + \delta\cosh[F(\phi_N - \phi_s)/RT]} \quad (4)$$

where $\phi_N = (RT/F)(pK - pH)\ln 10$ is the Nernst potential, $pK = (pK_{a1} + pK_{a2})/2$, and $\delta = 2\times 10^{-(pK_{a2} - pK_{a1})/2}$. $\phi_s$ is the surface potential. $e$ and $\Gamma$ are the elementary charge and the site density of the silanol group, respectively. The relation of the zeta potential ($\zeta$) and the surface potential is modeled by a basic Stern model:[45,46,52] $\zeta = \phi_s - \sigma/C_S$, where $C_S = \varepsilon_S\varepsilon_0/d_S$ is the capacitance of the Stern layer. $d_S$ is the Stern layer thickness of approximately the size of a water molecule (~0.3 nm). Because of the orientation of water molecules in the Stern layer, the reported dielectric constant of the Stern layer ($\varepsilon_S \approx 6$)[54] is much lower than the dielectric constant of bulk water. The electroneutrality condition of $\sigma + \sigma_d = 0$ holds in this model, where $\sigma_d$ is the charge density in the diffuse layer. It is noted that the surface binding reaction considered in the triple-layer model[55,56] was assumed to be neglected due to the low ionic strength (i.e., $I = 0.5\sum_i z_i^2 c_i$) in pure water or low salt solution. Note that the bulk ionic strength in our fluidic system was estimated to be on the order of micromoles per liter.

**Numerical Method.** The numerical results were obtained by solving the coupling of eqs 3 and 4. Equation 3 was discretized by a second-order accurate finite difference scheme with the point-successive-over-relaxation (PSOR) algorithm. The nonlinear term on the right-hand side of eq 3 was linearized by Taylor expansion. The numerical iterative procedure implemented to solve this nonlinear coupling model is addressed as follows: (1) initialization, give the parametric values of the PB equation and site-dissociation model and guess the initial value of $\sigma$ on channel walls; (2) do-loop, solve PB equation in eq 3 for $\zeta$ and $\phi$ and then solve eq 4 for $\phi_s$ and $\sigma$ using the Newton−Raphson method; (3) test, repeat the do-loop until $\sigma$ has converged. Once converged, this numerical procedure provides the EDL potential $\phi(y,z)$ for calculating the distribution of ions inside the nanochannels using eq 2. All numerical results presented in this study have been carefully checked to ensure that the solutions are grid independent. A nonuniform mesh of size 121 × 121 was used in our calculations. The minimum grid spacing in both the $y$- and $z$-directionsare less than 1 nm.

## RESULTS AND DISCUSSION

In our experiments, the pH value of the pure water mixed with fluorescein in the bulk or microchannel part is about 6 measured either by a pH meter or STED microscopy. According to this measured pH value, the bulk concentration of dissolved ions listed in Table 1 was calculated. The reported parameter values of the site density of silanol group ($\Gamma$) and the Stern layer capacitance ($C_S$) for silica surfaces are $\Gamma \approx 0.5-8$ sites/nm$^2$ and $C_S \approx 0.2-4.0$ F/m$^2$, respectively.[47−52] The exact parameter values for the silica nanochannel are very important but difficult to be determined in the numerical estimation because they vary with the silica type and its history. In our preliminary calculations, the reported data, $\Gamma = 8$/nm$^2$, $pK_{a2} = 7.9$, and $C_s = 0.3$ F/m$^2$,[29] for best fitting the streaming currents in 70−1147 nm depth fused-silica nanochannels of microscale width were used.

**Simulation with Bulk Water Property.** We assume that the dielectric constant of confined water within the diffuse layer is the same as the bulk ($\varepsilon_w = 79$) and has a uniform distribution. The calculated surface charge distribution on the wall of the nanochannel reveals a nonuniform distribution shown in Figure 2a, which is attributed to the corner-induced curvature effect on the EDL distribution in a nanochannel. Figure 2b shows the contour plot of the proton distribution within the diffuse layer in a nanochannel with a width of 410 nm and a depth of 405 nm. It is seen that EDL overlaps, and the proton concentration is the highest near the corner of the nanochannel. Figure 3 presents the comparisons of our experimental data[33] and the calculated results of the pH distribution ($pH = -\log c_{H^+}$). The numerical results are plotted across the centerline of the nanochannel. In Figure 3a, it can be seen that the result is very inconsistent with the experimental data. With increasing the $pK_{a2}$ value, the resulting profile of pH distribution does not seem to be consistent with the experimental data. Because the site density of the silanol group on the fused-silica surface may be changed after some physical and chemical treatments,[57] e.g., the nanofabrication and high-temperature thermal bonding processes for the nanochannel, Figure 3b shows the numerical results of pH distribution as a function of the silanol site density. The results are not shown to be agreement with the experimental data. We further change the value of the Stern layer capacitance to fit the experimental data, but it still fails because the calculated results are very weakly sensitive to the Stern layer capacitance, as shown in Figure 3c. Under the assumption of the bulk dielectric constant, the results calculated from various sets of the parameter values in the site-dissociation model always show a disagreement with experimental data. From eqs 2 and 3, it is seen that the ion distribution will be affected by the variation in


dx.doi.org/10.1021/ac400001v | Anal. Chem. 2013, 85, 4468−4474

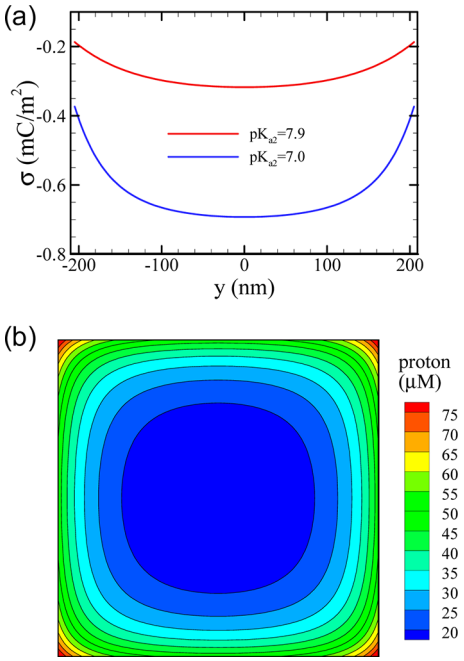


**Figure 2.** (a) Distribution of surface charge density along the wall of nanochannel with the different values of $pK_{a2}$. (b) Contour plot of proton distribution in nanochannel when the bulk dielectric constant of water ($\varepsilon_w$ = 79) was assumed. The parametric values of $\Gamma$ = 8/nm$^2$, $pK_{a2}$ = 7.9, and $C_s$ = 0.3 F/m$^2$ were used in the site-dissociation model.

temperature. However, the temperature variation in our experiments is very small (below 1.1 K)[39] and its effect on ion distribution can be reasonably ignored.

Accordingly, we infer that there are two possible reasons for this discrepancy: (1) the classical PB theory becomes invalid in nanochannel, and (2) the specific structure of water confined in nanochannels has a significant influence on the formation of EDL. In classical PB theory (weakly nonlinear theory), the ion was assumed as a point charge, while it fails at a very high zeta potential. Considering the ion size effect (or steric repulsion), the modified PB equation (strongly nonlinear theory) based on the mean-field theory has been proposed.[58,59] In general, the ion size effect becomes considerable when the zeta potential is higher than a critical potential, $|\zeta_c| \approx (RT/z_iF)\ \ln(c_{max}/c_i^{\infty})$, where $c_{max} = 1/N_A(2a_i)^3$ is a maximum local concentration of finite size ion ($N_A$ is the Avogadro constant and $a_i$ is the ion radius). For pure water with a pH value of 6.0 ($c_{H^+}^{\infty} = 10^{-6}$ M), the critical zeta potential $|\zeta_c| \approx 407$ mV is estimated (note that the hydronium radius is about 0.3 nm). Typically, the zeta potential of fused-silica surface is smaller than this critical value of $|\zeta_c| \approx 407$ mV. Therefore, it is considered that the ion size effect can be reasonably neglected, i.e., the classical PB theory based on point charge assumption is still valid in the extended nanochannels used in our study. In classical EDL theory, it is known that the Stern layer reveals a much lower permittivity than the diffuse layer due to the high electric field-induced orientation of water molecules within this immobile layer of about 0.3 nm.[54,60] The lower dielectric constant is expected to be around 6 for electrical saturation. Booth[61,62] has demonstrated that the water molecules become hardly polarized under a high electric field and reveals a lower permittivity than the bulk when the local electric field strength is larger than a critical value of $10^7$ V/m. However, except for the case of field-induced electrokinetics,[63] the local electric field

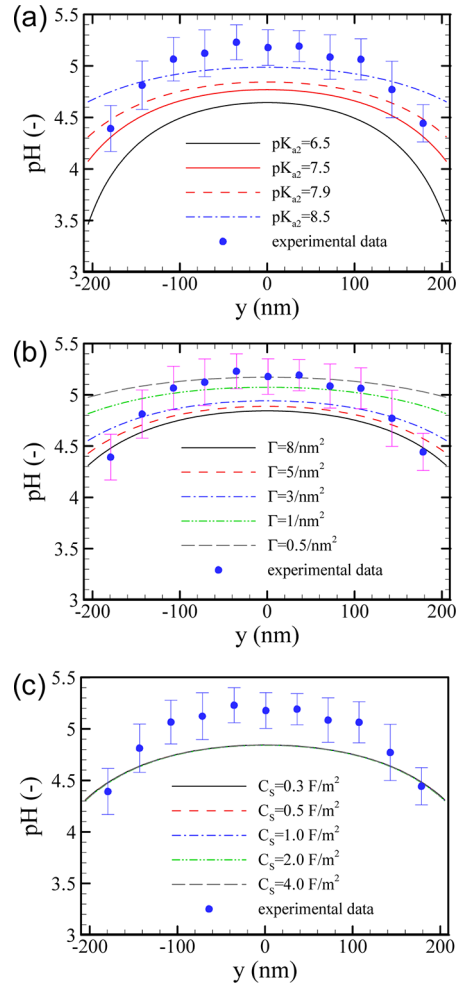


**Figure 3.** Comparison of the experimental result of pH distribution with the numerical results obtained from the PB theory and the site-dissociation model when the bulk dielectric constant of water ($\varepsilon_w$ = 79) was assumed. (a) Effect of $pK_a$ value of silanol group on pH distribution when $\Gamma$ = 8/nm$^2$ and $C_s$ = 0.3 F/m$^2$. (b) Effect of site density ($\Gamma$) of silanol group on pH distribution when $pK_{a2}$ = 7.9 and $C_s$ = 0.3 F/m$^2$. (c) Effect of Stern layer capacitance ($C_S$) on pH distribution when $\Gamma$ = 8/nm$^2$ and $pK_{a2}$ = 7.9.

within the diffuse layer generally is much smaller than this critical value and therefore the bulk water permittivity is reasonably assumed within this layer. However, it should be noted that the classical EDL theory discussed above was considered as a charge distribution at an interface region in homogeneous liquid that is approximated to be the liquid at infinity. From our recent studies,[18−22] we have suggested an importance of the heterogeneous liquid structure at the interface region in fused-silica extended nanochannels, i.e., a three-phase model for water confined in extended nanochannels. In other words, we infer that the assumption of bulk properties such as ion diffusivity, ion mobility, and water permittivity may become invalid in the diffuse layer because the structural water is expected under the confinement and surface effects. According to the Nernst−Planck equation: $\mathbf{j}_i = -m_i c_i \nabla\psi - D_i \nabla c_i$,[23] it is known that the ion flux ($\mathbf{j}_i$) is influenced by the ion diffusivity ($D_i$) and mobility ($m_i$). Consider the Nernst−Einstein relation: $D_i = RT/z_iF$,[23] the ion flux can be rewritten as $\mathbf{j}_i = -(z_iF/RT)D_i c_i \nabla\phi - D_i \nabla c_i$. Under the condition of zero-flux normal to the channel wall (i.e., $\mathbf{j}_i \cdot \mathbf{n} = 0$), the ion reveals a


dx.doi.org/10.1021/ac400001v | Anal. Chem. 2013, 85, 4468−4474

Boltzmann distribution as eq 2. It implies that the influences of ion diffusivity and mobility on ion distribution can be reasonably neglected even if the ion diffusivity and mobility in extended nanochannels are changed due to the structural water. Accordingly, it is inferred that the specific water permittivity due to the specific structure of water molecules has an influence on the ion distributions in extended nanochannels.

**Simulation with Specific Water Property.** On the basis of our proposed "three-phase model" for the heterogeneous water structure in extended nanochannels,[18,19] it is expected that the permittivity of confined water will reveal a nonuniform distribution in a fused-silica extended nanochannel. The more oriented water structure close to the wall reveals a much lower permittivity. It can be inferred that the water structure in the adsorbed phase of about 1 nm is similar to ice, having a bilayer structure where both translation and rotation of water molecules are inhibited and reveals the lowest permittivity. In the proton-transfer phase of approximately 50 nm,[19] the surface and size-confinement effects on the translational motion of water molecules imply that it may have a lower permittivity than the bulk phase. However, it is very difficult to determine the exact permittivity distribution in an extended nanochannel. Herein we infer that the proton-transfer phase becomes dominant when the diffuse layer thickness (Debye length) is of the order of 100 nm. Then, the effective permittivity of confined water with a uniform distribution across the diffuse layer was assumed for our present calculations. Figure 4 shows

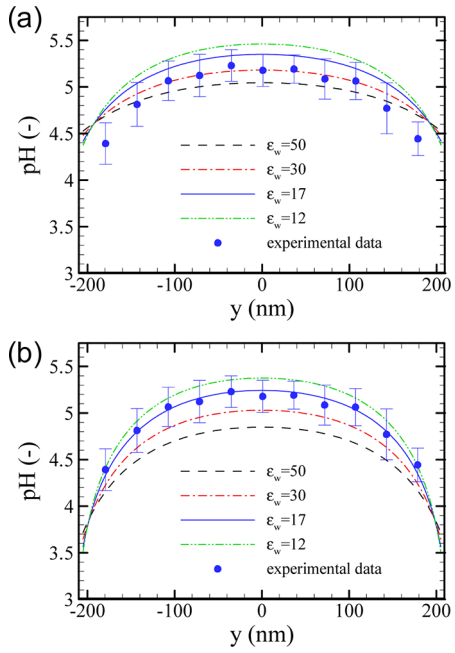


**Figure 4.** Effect of the dielectric constant of water confined in a nanochannel on pH distribution for two different values of (a) $pK_{a2}$ = 7.9 and (b) $pK_{a2}$ = 6.5. The parametric values of $\Gamma$ = 3/nm$^2$ and $C_s$ = 0.2 F/m$^2$ are kept constant in the calculations.

the numerical results of pH distribution as a function of the effective dielectric constant of confined water for two different $pK_{a2}$ values of the silanol group. Note that the silanol site density of about 3/nm$^2$ on the fused-silica surface suggested by the Scales et al.[60] was used in our calculations. The Stern layer capacitance of 0.2 F/m$^2$ estimated with $d_S \approx 0.3$ nm and $\varepsilon_S \approx 6$ was assumed.[54] It is seen that the numerical results with $pK_{a2}$ = 7.9 in Figure 4a are not in agreement with the experimental data for any dielectric constants, while the calculated result of $pK_{a2}$ = 6.5 with a lower dielectric constant of approximately 17 in Figure 4b shows good agreement with the experimental data. This lower dielectric constant of 17 is very close to the value of one-seventh of bulk dielectric constant (∼12) estimated from our previous time-resolved fluorescence measurements in 300 nm fused-silica extended nanochannels.[21] The lower dielectric constant of confined water indicates that the Debye length,[60] $\lambda_D = (\varepsilon_w\varepsilon_0 RT/F^2 \sum_i z_i^2 c_i^\infty)^{1/2}$, becomes thinner in extended nanochannels. In addition, the Gouy−Chapmann length,[64] $\lambda_{GC} = 2\varepsilon_w\varepsilon_0 RT/zF|\sigma|$, defining a layer within which the most counterions (hydronium ions for pure water) are located, also becomes smaller due to the lower permittivity of water confined in nanochannels, as shown in Figure 4b. It is found that the zeta potential estimated from eq 2 is approximately −150 mV. Further, the influence of the $pK_{a2}$ value on the pH distribution is presented in Figure 5a. The calculated results of the lower $pK_{a2}$ value are shown to be more consistent with the experimental data. It is suggested that the silanol group has a

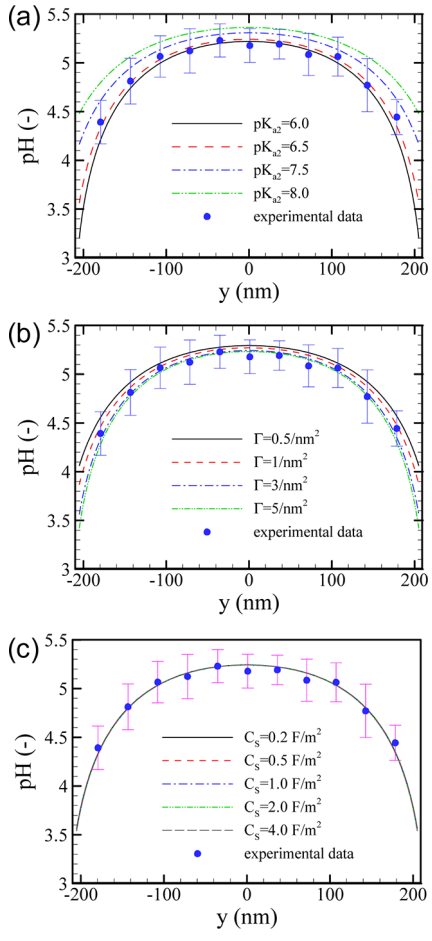


**Figure 5.** Comparison of the experimental result of pH distribution with the numerical results obtained from the PB theory and the site-dissociation model when the lower dielectric constant of confined water ($\varepsilon_w$= 17) was assumed. (a) Effect of $pK_{a2}$ value of the silanol group on the pH distribution when $\Gamma$ = 3/nm$^2$ and $C_s$ = 0.2 F/m$^2$. (b) Effect of site density ($\Gamma$) of the silanol group on the pH distribution when $pK_{a2}$ = 6.5 and $C_s$ = 0.2 F/m$^2$. (c) Effect of the Stern layer capacitance on the pH distribution when $\Gamma$ = 3/nm$^2$ and $pK_{a2}$ = 6.5.


dx.doi.org/10.1021/ac400001v | Anal. Chem. 2013, 85, 4468−4474

higher deprotonation rate in extended nanochannels, which confirms our previous experimental observation that the shift of the PZC of the silanol group occurs in sub-800 nm nanochannels.[38] This result is also supported by our previous NMR study that the fast proton-transfer rate induced by chemical exchange between water molecules and the silanol group was observed in sub-800 nm fused-silica nanochannels.[18,19] The effect of silanol site density shown in Figure 5b reveals a little bit of an influence on the proton distribution within the reasonable range of silanol site density on fused-silica surfaces. The best fitting value of silanol site density was found to be 3−5/nm$^2$, which is very consistent with the reported site density for the fused-silica surface.[34,47−51,56] The influence of the Stern layer capacitance was further considered in our calculations, and the indistinguishable calculated results indicated the proton distribution within the diffuse layer is insensitive to the Stern layer capacitance, as shown in Figure 5c.

As discussed above, an emerging question is Why does the water confined in fused-silica nanochannels reveal a lower dielectric constant? In the bulk phase, it is well-known that the dielectric saturation due to the orientation of the water dipole around the ions decreases their rotational degrees of freedom and then reduces the dielectric constant at the high salt concentration.[65] However, the various ion concentrations (e.g., $H_3Fl^+$, $HFl^-$, and $Fl^{2-}$) in our fluidic system all were estimated to be very dilute (less than 1 $\mu$M). Therefore, the decrease in the water dielectric constant due to the dielectric saturation is reasonably assumed to be negligible in our fluidic system. On the other hand, we anticipate that the orientational structure of confined water molecules due to the confinement and surface effects will result in the specific behavior of water. The hydrogen bonding network is expected to be well-developed due to the effects of the size-confinement and the charged silanol group in silica nanochannels. As a result, the dielectric polarization of water molecules confined in nanochannels may be suppressed, i.e., the magnitude of the dipole moment of the water molecules becomes smaller. Many molecular dynamics (MD) simulations have demonstrated that the dielectric constant of water confined in nanospaces is lower than the bulk system. For example, Zhang et al.[66] reported that water confined in spherical cavity with a diameter of 2.7 nm has a much smaller dielectric constant of about 5 than the bulk due to the presence of a structural ordering of about two to three molecular layers of water at the surface. Senapati and Chandra[67] demonstrated that the water in a sub-2 nm nanoconfinement reveals a nearly 50% decrease of the dielectric constant. In the absence of the surface functional group, the decrease in the dielectric constant of water was attributed to the pure confinement effect. More recently, Zhu et al.[68] implemented the MD simulations of water and salt solutions in a 2.4 nm hydrophilic silica nanopore to study the dielectric behavior of nanoconfined salt solutions, but the effect of silica surface properties on the dielectric properties of confined water was not discussed. A dramatic decrease in dielectric constant of pure water perpendicular to the walls ($\varepsilon_w^{\perp}$) was observed in their simulations, while an unexpected increase in $\varepsilon_w^{\perp}$ of salt solution at a critical salt concentration was found due to an interplay between the effects of confinement and salt ions on the water hydrogen bonding network. However, these MD simulations were all implemented in sub-10 nm nanospaces and not extended nanospaces. The more exact mechanism for the specific properties of water confined in the hydrophilic silica extended nanochannel remains unclear. On the basis of our NMR observations of water dynamics in silica extended nanochannels, a hypothesized "proton-transfer phase" between the adsorbed water phase and bulk water phase was proposed to preliminarily explain why the confined water reveals the specific behaviors.[18,19] In this intermediate phase, the water molecules have more complicated properties than the others, e.g., the water molecules preserve the four-coordinate $H_2O$ structure, a slower motion of water molecules than the bulk, a size confinement effect only on the intermolecular translation without changes in the rotation, and proton hopping along a hydrogen-bond chain. In other words, the water molecules in this phase form a loosely structured water network by a hydrogen bond within approximately 50 nm from the water/silica interface in extended nanochannels. This specific structure and behavior of water molecules has been further demonstrated by observations of higher proton mobility[20] and higher water viscosity[21,22] in fused-silica extended nanochannels. Here we anticipate that this loosely structured water network reveals a very different dielectric behavior from the bulk water. Note that the size-confinement and surface effects on the behaviors of liquid molecules were distinctly observed for protic solvents confined in fused-silica extended nanochannels, while they did not appear for aprotic and nonpolar solvents.[18] As a result, we infer that the dielectric behavior of confined aprotic solvent may not be different from the bulk and does not affect the charge distribution.

## CONCLUSIONS

We have presented comparisons of numerical and experimental results of the proton distribution to investigate the effect of specific water properties on the formation of EDL in a fused-silica extended nanochannel. On the basis of the PB theory combined with the silanol site-dissociation model, the results indicated that (1) the PB theory still is valid in extended nanochannels but the specific water properties should be considered, (2) the water confined in extended nanochannels reveals a lower permittivity, and (3) the silanol group in extended nanochannels reveals a higher deprotonation rate. The effective dielectric constant of water within the diffuse layer in a 410 nm nanochannel was estimated to be 17, which is close to the reported value of one-seventh of the bulk dielectric constant (~12) in 330 nm nanochannels estimated from the time-resolved fluorescence measurements.[21] The higher silanol deprotonation rate found in silica extended nanochannels confirms our previous observations showing a shift of the PZC of the silanol group[38] and a higher proton exchange rate between the silanol group and the water molecules[18,19] in sub-800 nm fused-silica nanochannels. These specific features in fused-silica extended nanochannels are supported by the hypothetical model of a proton-transfer phase between the adsorbed phase and the bulk phase,[18,19] in which the water molecules form a loosely structured water by the hydrogen bonding network. The present study provides useful information for further understanding the EDL-related transport phenomena at the nanoscale, which plays an important role in microanalytical chemistry, soil science, energy harvesting, and biology as well as in biological and energy conversion processes such as ionic transport in membranes. Our future work will focus on the direct measurements of more exact dielectric behavior of water confined in fused-silica extended nanochannels.


dx.doi.org/10.1021/ac400001v | Anal. Chem. 2013, 85, 4468−4474

## AUTHOR INFORMATION


### Corresponding Author

*Phone: +81-3-5841-7231. Fax: +81-3-5841-6039. E-mail: kitamori@icl.t.u-tokyo.ac.jp.


### Notes

The authors declare no competing financial interest.

## ACKNOWLEDGMENTS


Chih-Chang Chang and Ruey-Jen Yang gratefully acknowledge the financial support provided to this work by the National Science Council (NSC) of Taiwan under Grant No. NSC-99-2221-E-006-079-MY3 and the NCKU Academic Summit Program. This work was also supported by a Grant-in-Aid for Specially Promoted Research from the Japan Society for the Promotion of Science (JSPS).


## REFERENCES


(1) Eijkel, J.; van den Berg, A. *Microfluid. Nanofluid.* **2005**, *1*, 249.
(2) Schoch, R. B.; Han, J.; Renaud, P. *Rev. Mod. Phys.* **2008**, *80*, 839.
(3) Tsukahara, T.; Mawatari, K.; Kitamori, T. *Chem. Soc. Rev.* **2010**, *39*, 1000.
(4) Siwy, Z. S.; Howorka, S. *Chem. Soc. Rev.* **2010**, *39*, 1115.
(5) Hou, X.; Guo, W.; Jiang, L. *Chem. Soc. Rev.* **2011**, *40*, 2385.
(6) Humplik, T.; Lee, J.; O'Hern, S. C.; Fellman, B. A.; Baig, M. A.; Hassan, S. F.; Atieh, M. A.; Rahman, F.; Laoui, T.; Karnik, R.; Wang, E. N. *Nanotechnology* **2011**, *22*, 292001.
(7) Liu, S.; Pu, Q.; Gao, L.; Korzeniewski, C.; Matzke, C. *Nano Lett.* **2005**, *5*, 1389.
(8) van der Heyden, F. H. J.; Bonthuis, D. J.; Stein, D.; Meyer, C.; Dekker, C. *Nano Lett.* **2007**, *7*, 1022.
(9) Chang, C.-C.; Yang, R.-J. *Appl. Phys. Lett.* **2011**, *99*, 083102.
(10) Koga, K.; Gao, G. T.; Tanaka, H.; Zeng, X. C. *Nature* **2001**, *412*, 802.
(11) Farrer, R. A.; Fourkas, J. T. *Acc. Chem. Res.* **2003**, *36*, 605.
(12) Milischuk, A. A.; Ladanyi, B. M. *J. Chem. Phys.* **2011**, *135*, 174709.
(13) Le Caër, S.; Lima, M.; Gosset, D.; Simeone, D.; Bergaya, F.; Pommeret, S.; Renault, J.-Ph.; Righini, R. *J. Phys. Chem. C* **2012**, *116*, 12916.
(14) Alabarse, F. G.; Haines, J.; Cambon, O.; Levelut, C.; Bourgogne, D.; Haidoux, A.; Granier, D.; Coasne, B. *Phys. Rev. Lett.* **2012**, *109*, 035701.
(15) Duan, C.; Majumdar, A. *Nat. Nanotechnol.* **2010**, *5*, 851.
(16) Persson, F.; Tegenfeldt, J. O. *Chem. Soc. Rev.* **2010**, *39*, 985.
(17) Levy, S. L.; Craighead, H. G. *Chem. Soc. Rev.* **2010**, *39*, 1133.
(18) Tsukahara, T.; Hibara, A.; Ikeda, Y.; Kitamori, T. *Angew. Chem., Int. Ed.* **2007**, *46*, 1180.
(19) Tsukahara, T.; Mizutani, W.; Mawatari, K.; Kitamori, T. *J. Phys. Chem. B* **2009**, *113*, 10808.
(20) Chinen, H.; Mawatari, K.; Pihosh, Y.; Morikawa, K.; Kazoe, Y.; Tsukahara, T.; Kitamori, T. *Angew. Chem., Int. Ed.* **2012**, *51*, 3573.
(21) Hibara, A.; Saito, T.; Kim, H.; Tokeshi, M.; Ooi, T.; Nakao, M.; Kitamori, T. *Anal. Chem.* **2002**, *74*, 6170.
(22) Li, L.; Kazoe, Y.; Mawatari, K.; Sugii, Y.; Kitamori, T. *J. Phys. Chem. Lett.* **2012**, *3*, 2447.
(23) Probstein, R. F. *Physicochemical Hydrodynamics: An Introduction*, 2nd ed.; John Wiley & Sons: New York, 1994.
(24) Pu, Q. S.; Yun, J. S.; Temkin, J.; Liu, S. R. *Nano Lett.* **2004**, *4*, 1099.
(25) Kim, S. J.; Wang, Y.-C.; Lee, J. H.; Jang, H.; Han, J. *Phys. Rev. Lett.* **2007**, *99*, 044501.
(26) Karnik, R.; Duan, C.; Castelino, K.; Daiguji, H.; Majumdar, A. *Nano Lett.* **2007**, *7*, 547.
(27) Vlassiouk, I.; Siwy, Z. S. *Nano Lett.* **2007**, *7*, 552.
(28) Cheng, L.-J.; Guo, L. J. *Nano Lett.* **2007**, *7*, 3165.
(29) van der Heyden, F. H. J.; Stein, D.; Dekker, C. *Phys. Rev. Lett.* **2005**, *95*, 116104.
(30) Chang, C.-C.; Yang, R.-J. *J. Colloid Interface Sci.* **2009**, *339*, 517.
(31) Morikawa, K.; Mawatari, K.; Kato, M.; Tsukahara, T.; Kitamori, T. *Lab Chip* **2010**, *10*, 871.
(32) Andersen, M. B.; Bruus, H.; Bardhan, J. P.; Pennathur, S. *J. Colloid Interface Sci.* **2011**, *360*, 262.
(33) Wang, M.; Kang, Q.; Ben-Naim, E. *Anal. Chim. Acta* **2010**, *664*, 15.
(34) Jensen, K. L.; Kristensen, J. T.; Crumrine, A. M.; Andersen, M. B.; Bruus, H.; Pennathur, S. *Phys. Rev. E* **2011**, *83*, 056307.
(35) Stein, D.; Kruithof, M.; Dekker, C. *Phys. Rev. Lett.* **2004**, *93*, 035901.
(36) Pennathur, S.; Santiago, J. G. *Anal. Chem.* **2005**, *77*, 6772.
(37) Pennathur, S.; Santiago, J. G. *Anal. Chem.* **2005**, *77*, 6782.
(38) Morikawa, K.; Mawatari, K.; Kazoe, Y.; Tsukahara, T.; Kitamori, T. *Appl. Phys. Lett.* **2011**, *99*, 123115.
(39) Kazoe, Y.; Mawatari, K.; Sugii, Y.; Kitamori, T. *Anal. Chem.* **2011**, *83*, 8152.
(40) Anzo, K.; Okada, T. *Anal. Chem.* **2012**, *84*, 10852.
(41) Kazoe, Y.; Chang, C.-C.; Mawatari, K.; Kitamori, T. *Anal. Chem.* **2012**, *84*, 10855.
(42) Chang, C.-C.; Yang, R.-J.; Wang, M.; Miau, J.-J.; Lebiga, V. *Phys. Fluids* **2012**, *24*, 072001.
(43) Baldessari, F.; Santiago, J. G. *J. Colloid Interface Sci.* **2008**, *325*, 526.
(44) Diehl, H.; Markuszewski, R. *Talanta* **1985**, *32*, 159.
(45) Hiemstra, T.; Van Riemsdijk, W. H.; Bolt, G. H. *J. Colloid Interface Sci.* **1989**, *133*, 91.
(46) Hiemstra, T.; De Wit, J. C. M.; Van Riemsdijk, W. H. *J. Colloid Interface Sci.* **1989**, *133*, 105.
(47) Iler, R. K. *The Chemistry of Silica*; John Wiley & Sons: New York, 1979.
(48) van Hal, R. E. G.; Eijkel, J. C. T.; Bergveld, P. A. *Adv. Colloid Interface Sci.* **1996**, *69*, 31.
(49) Ong, S.; Zhao, X.; Eisenthal, K. B. *Chem. Phys. Lett.* **1992**, *191*, 327.
(50) Scales, P. J.; Grieser, F.; Healy, T. W.; White, L. R.; Chan, D. Y. C. *Langmuir* **1992**, *8*, 965.
(51) Sonnefeld, J. *J. Colloid Interface Sci.* **1996**, *183*, 597.
(52) Behrens, S. H.; Grier, D. G. *J. Chem. Phys.* **2001**, *115*, 6716.
(53) Healy, T. W.; White, L .R. *Adv. Colloid Interface Sci.* **1978**, *9*, 303.
(54) Hiemstra, T.; Van Riemsdijk, W. H. *Colloids Surf.* **1991**, *59*, 7.
(55) Wang, M.; Revil, A. *J. Colloid Interface Sci.* **2010**, *343*, 381.
(56) Andersen, M. B.; Frey, J.; Pennathur, S.; Bruus, H. *J. Colloid Interface Sci.* **2011**, *353*, 301.
(57) Yates, D. E.; Healy, T. W. *J. Colloid Interface Sci.* **1976**, *55*, 9.
(58) Borukhov, I.; Andelman, D.; Orland, H. *Phys. Rev. Lett.* **1997**, *79*, 435.
(59) Kilic, M. S.; Bazant, M. Z.; Ajdari, A. *Phys. Rev. E* **2007**, *75*, 021502.
(60) Hunter, R. J. *Zeta Potential in Colloid Science*; Academic Press: New York, 1981.
(61) Booth, F. *J. Chem. Phys.* **1951**, *19*, 391.
(62) Booth, F. *J. Chem. Phys.* **1955**, *23*, 453.
(63) Bazant, M. Z.; Kilic, M. S.; Storey, B.; Ajdari, A. *New J. Phys.* **2009**, *11*, 075016.
(64) Bocquet, L.; Charlaix, E. *Chem. Soc. Rev.* **2010**, *39*, 1073.
(65) Marcus, Y. *Chem. Rev.* **2011**, *111*, 2761.
(66) Zhang, L.; Davis, H. T.; Kroll, D. M.; White, H. S. *J. Phys. Chem.* **1995**, *99*, 2878.
(67) Senapati, S.; Chandra, A. *J. Phys. Chem. B* **2001**, *105*, 5106.
(68) Zhu, H.; Ghoufi, A.; Szymczyk, A.; Balannec, B.; Morineau, D. *Phys. Rev. Lett.* **2012**, *109*, 107801.